ISSN:2584-2706 DOI: https://doi.org/10.67317/IJMSRT26AUG180

Voltage Stability and Transient Response Assessment of a Hybrid Renewable-Integrated Nigerian 330-kV Grid: A Static and Dynamic Analysis

*Muibi K. A; Aizenofe, M. O; Ibrahim, S. A
Department of Electrical and Electronics Engineering, School of Engineering,
Yaba College of Technology, Yaba, Lagos State, Nigeria

Olatidoye, K. G
Electrical Maintenance Section, Works and Services, Yaba College of
Technology, Yaba, Lagos State, Nigeria

***Corresponding Author**

Abstract
The aggressive penetration of Hybrid Renewable Energy Sources (HRES) into weak transmission network creates challenges in voltage regulation and transient stability. This paper examines the impact of high penetration of photovoltaic (PV) and wind energy on the voltage stability and transient response of the Nigerian 330-kV, 34-bus transmission network. Newton-Raphson power flow and Continuation Power Flow (CPF) methods are used to find the voltage collapse proximity and loadability limits for determining the static stability. For the dynamic analyses, time domain simulations are used to assess rotor angle and speed deviations following critical three-phase faults. Further, the performance of Flexible AC Transmission Systems (FACTS) devices, namely the Thyristor-Controlled Series Capacitor (TCSC) and Static Synchronous Compensator (STATCOM) in reducing the instability is comparatively analysed. The results show that the base network experiences severe voltage deficiencies at the remote busses (Gombe: 0.907 p.u., Jos: 0.949 p.u.) and is vulnerable to cascading failures under contingencies. The inclusion of HRES makes the instability worse and the critical clearing times are violated. However, the best position of STATCOM shows a better performance than TCSC in restoring the Gombe bus voltage from 0.907 p.u. to 1.049 p.u. and maintaining the transient stability margins. These findings provide a framework for grid operators to reinforce weak networks undergoing renewable energy transition.

Keywords:
Voltage stability; Transient stability; Hybrid renewable energy; FACTS devices; Continuation power flow.

1. Introduction

The global decarbonization transition has resulted in an increased penetration of variable renewable energy sources (VRES) such as solar photovoltaic (PV) and wind turbines into conventional power systems [1]. The grid infrastructure in developing countries such as Nigeria is characterized by long transmission distances, inadequate reactive power compensation and limited spinning reserves. This creates a complex stability problem for the injection of non-synchronous generation [2], [3]. The Nigerian 330 kV transmission network, the backbone of the national grid, is well known to have

ISSN:2584-2706 DOI: https://doi.org/10.67317/IJMSRT26AUG180

structural weaknesses. Such as low voltage profile at load centres and vulnerability to voltage collapse during peak demand or contingencies [4], [5].

The intermittent nature of wind and solar resources leads to more complex power flows which can reduce the system inertia and damping ability, and threaten both small-signal and transient stability [6], [7]. The integration of renewable energy sources is vital to address the energy requirements of the country and reduce the carbon footprints, but it demands a comprehensive assessment of static and dynamic stability margins to prevent cascading failures [8].

Static voltage stability analysis (namely Continuation Power Flow (CPF)) is of particular importance to evaluate the proximity to voltage collapse and to identify critical busses [9]. In contrast, transient stability analysis studies the ability of the system to remain in synchronism after severe disturbances such as three phase faults which are prevalent in the Nigerian grid [10]. To address these problems, FACTS controllers such as shunt-connected STATCOM and series-connected TCSC have been proposed for voltage support and power flow control [11], [12].

Several studies [2], [13] have examined renewable integration in Nigeria, but detailed analyses on static voltage collapse phenomena and transient rotor dynamics with hybrid renewable penetration simultaneously are still scarce. Also, there are no comparative studies on the application of FACTS devices that are specifically designed for the topology of the Nigerian network.

This paper fills this gap by presenting a detailed static and dynamic stability assessment of the Nigerian 330-kV grid with integrated PV and Doubly-Fed Induction Generator (DFIG) based wind farms. The specific aims are to (i) identify the weak busses and voltage collapse points through CPF and eigenvalue analysis, (ii) evaluate the transient stability through rotor angle and speed responses under critical fault conditions and (iii) determine the optimal compensation strategy through STATCOM and TCSC to improve the system resilience.

Figure 1: Single-Line Diagram

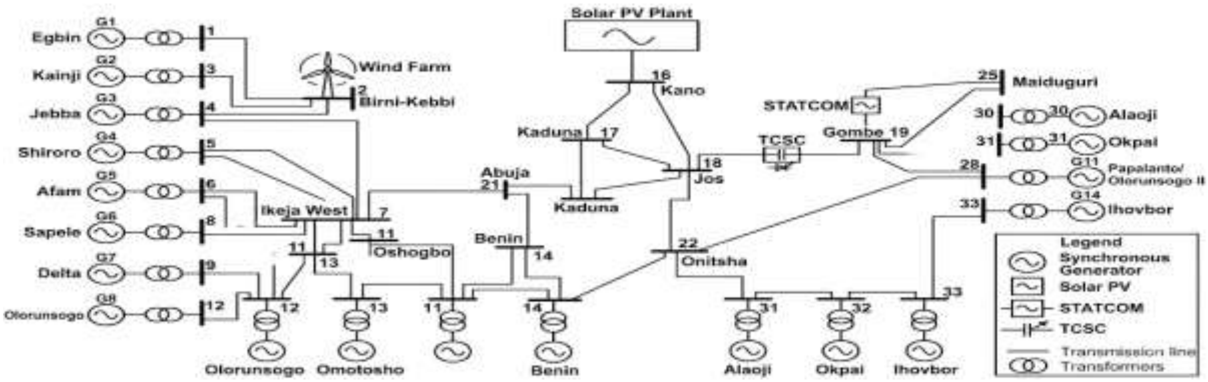

Figure 2: Methodology Flowchart

ISSN:2584-2706 DOI: https://doi.org/10.67317/IJMSRT26AUG180

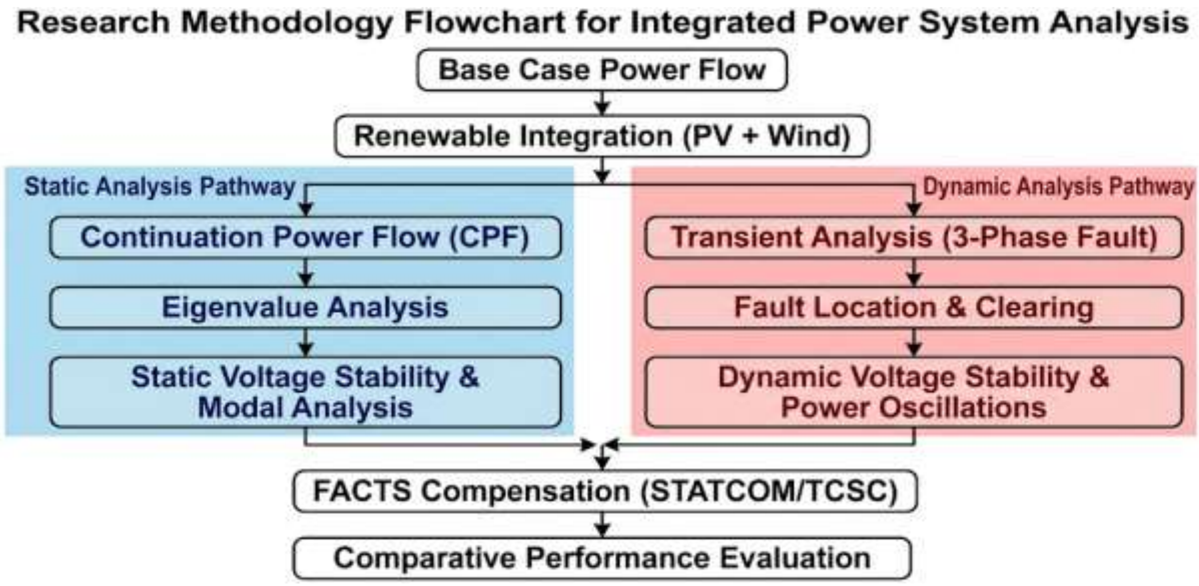

2. System Modelling and Methodology

2.1 Network Configuration and Base Case

The transmission network used in this study is the Nigerian 330-kV 34-bus 14 synchronous generator transmission network. It forms the backbone of the Nigerian national grid with a radial topology and long power transfer distances between generation centres in the south and load centres in the north [14]. The full Newton-Raphson method is used to solve the base case load flow. The base case load flow is solved with Egbin Power Station (Bus 22) as the slack bus because it is the largest generating station (700 MW capacity) for active and reactive power balance [15].

Base values for per unit normalization are 100 MVA and 330 kV. The network data such as line impedances, generation schedules and load profiles are adapted from the Nigerian Transmission Company (TCN) operational records and validated against literature [4], [16]. The modified network includes a 240 MW Wind Energy System (WES) at Binni-Kebbi Bus (Bus 11) and a 150 MW Solar PV farm at Kano Bus (Bus 13) based on the optimal availability of renewable resources (wind speed of 4.476 m/s and solar irradiance of 1,815 kWh/kWp, respectively) [17], [18].

Figure 3: Network Topology

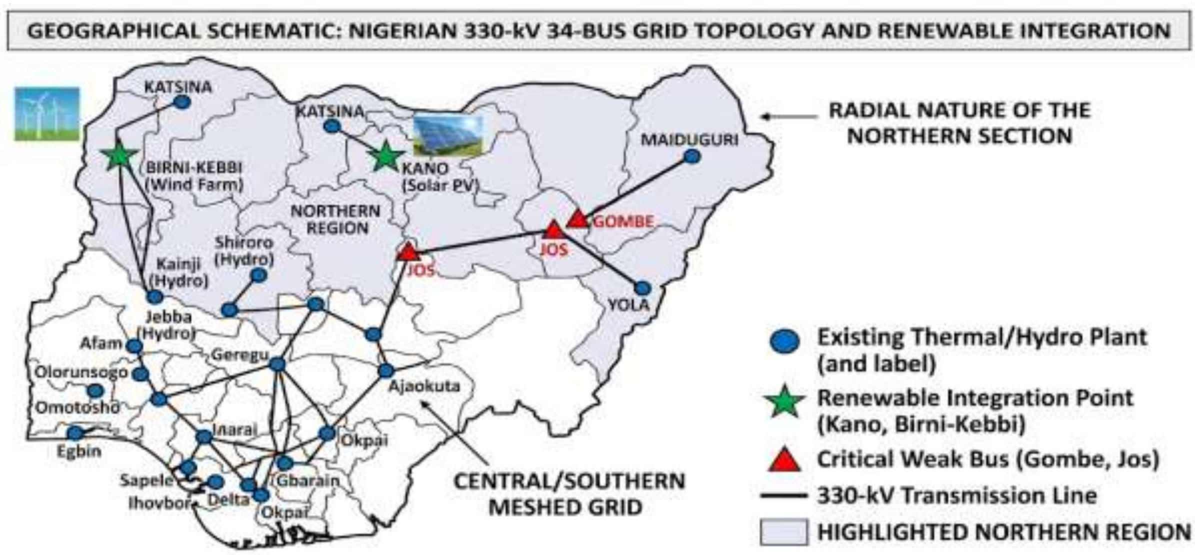

ISSN:2584-2706 DOI: https://doi.org/10.67317/IJMSRT26AUG180

2.2 Renewable Energy Source Modelling

2.2.1 DFIG-Based Wind Energy Conversion System

The wind farm is modelled as a Doubly-Fed Induction Generator (DFIG) (Type 3 wind turbine). The DFIG configuration is one of the most common in modern wind farms because it can operate at variable speeds (±33% of synchronous speed) and decouple the control of active and reactive power [19]. The DFIG stator is directly connected to the grid, while the rotor windings interface via a back-to-back Voltage Source Converter (VSC).

The power flow equations for the DFIG, neglecting stator resistance, are given by [20]:

$Ps = vds\ ids + vqs\ iqs (1)$

$Qs = vqs\ ids - vds\ iqs (2)$

Where Ps and Qs are stator active and reactive power respectively and vds, vqs, ids, iqs are the direct and quadrature axis components of stator voltage and current. The total injected power is equal to the sum of power injection into rotor and stator Pr+ Ps. In studies of power flow, the wind farm is modelled as a single equivalent PV generator connected at the point of common coupling, with real power injection, derived from the Weibull wind speed distribution and turbine power curve [21].

2.2.2 Photovoltaic System Model

The solar PV farm is modelled as a current source drawn power to the grid. By using the single-diode model [22], the basic I-V characteristics of the PV array are obtained:

$I = Ipv, cell - I_0, cell[exp(qV/aKT) - 1] (3)$

Where Ipv, cell is the photogenerated current, I_0, cell the reverse saturation current, q the electron charge, K the Boltzmann's constant, T the cell temperature and a the diode ideality factor. The array configuration (series/parallel modules) defines the system's total voltage and current. In stability studies, the PV system is modelled as a negative load (power injection) with unity power factor operation, according to modern grid codes that use inverters for reactive power support [23].

Figure 4: Renewable Energy Equivalent Circuits

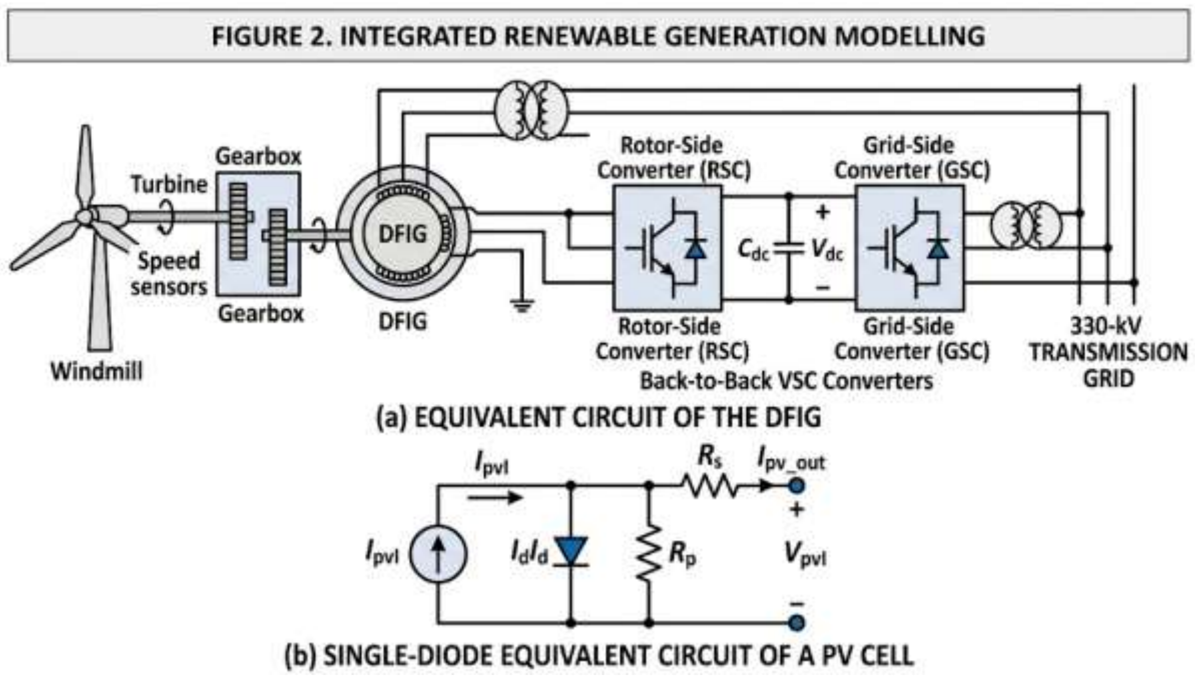

2.3 FACTS Controllers

Based on voltage sensitivity analysis, two FACTS devices are optimally placed to damp voltage instability and improve transient response:

2.3.1 STATCOM Model

ISSN:2584-2706 DOI: https://doi.org/10.67317/IJMSRT26AUG180

The Static Synchronous Compensator (STATCOM) is modelled as a shunt connected Voltage Source Converter (VSC) which behaves as a synchronous voltage source**.** It provides dynamic reactive power compensation according to:

$$Q_{STATCOM} = \frac{V_{sh}^2 + V_{sh}V_{bus}\cos(\delta_{sh} - \delta_{bus})}{X_{sh}}$$

where Vsh and δsh are the magnitude and angle of the injected voltage, and Xsh is the coupling reactance. The controller is placed at Gombe Bus (Bus 17), identified as the weakest bus in the CPF analysis (voltage 0.907 p.u.), to provide local voltage support [24].

2.3.2 TCSC Model

The Thyristor-Controlled Series Capacitor (TCSC) is modelled as a variable reactance XTCSC inserted in series with the transmission line between Gombe and Jos. The effective line reactance becomes Xline−XTCSC, enhancing power transfer capability and voltage regulation. The compensation level is set to 200% of the line reactance to maximize power flow control [25].

Figure 5: FACTS Integration Schematic

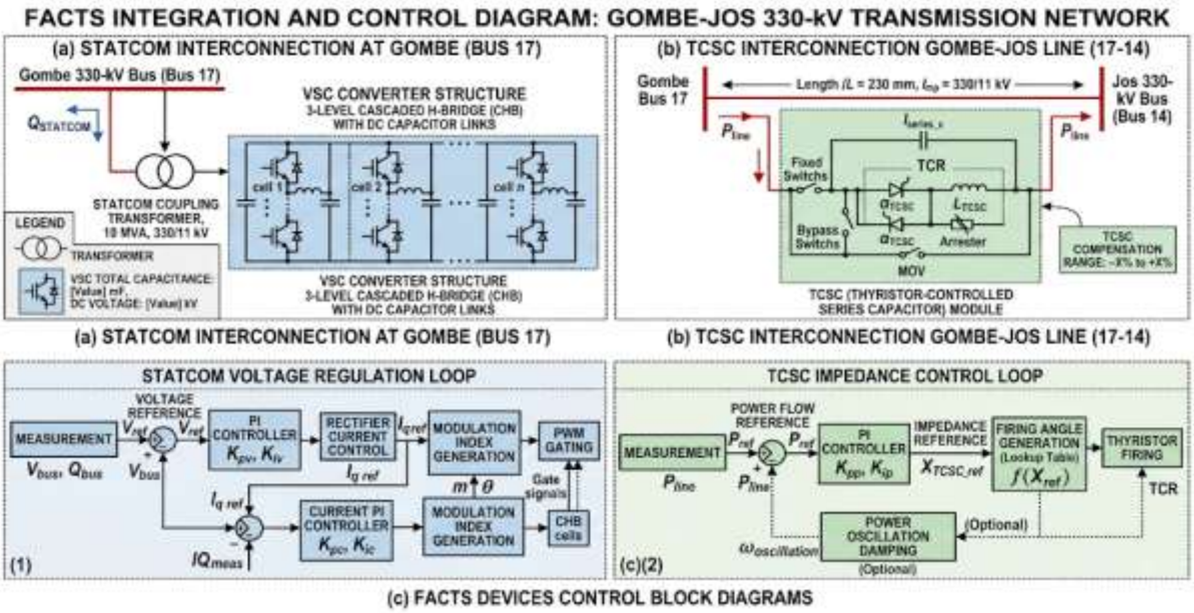

.

2.4 Static Stability Assessment Methodology

The static voltage stability is evaluated through three sequential analyses:

1. Newton-Raphson Power Flow: Gives the base operating point, and the initial voltage profile. Convergence is met when power mismatches are less than 10−6 p.u. [26].
2. Continuation Power Flow (CPF): Solves the singularity of the Jacobian matrix near to voltage collapse using a predictor-corrector scheme. The loading parameter λ is gradually increased until the critical point (saddle-node bifurcation) is reached where $d\lambda/dV = 0$ [27]. The P-V curve nose point indicates the maximum loadability margin.
3. Eigenvalue Analysis: The reduced Jacobian matrix (JRJR) obtained from the power flow solution is used to detect the participation factors and instability modes. Small-signal stability: any eigenvalue has negative real part [28].

2.5 Transient Stability Assessment Methodology

Transient stability is evaluated using time-domain simulation in PSAT/MATLAB. The synchronous generators are modelled with detailed sub-transient dynamics (two-axis model) including automatic voltage regulators (AVR) and turbine governors [29]. The simulation procedure involves:

1. **Initialization**: Steady-state operating point established via power flow.

2. **Fault Application**: A three-phase short-circuit fault is applied at critical buses (Jos and Kano) for duration t_{fault} = 0.1s (5 cycles), cleared at t_{clear} = 2.1s with line isolation.
3. **Monitoring**: Rotor angles (δ) and speeds (ω) of all synchronous generators are monitored for 10 seconds post-fault to assess synchronism retention. Instability is declared if any generator's rotor angle exceeds 180∘180∘ relative to the centre of inertia or if speed deviations persist without damping [30].

Figure 6: Simulation Framework

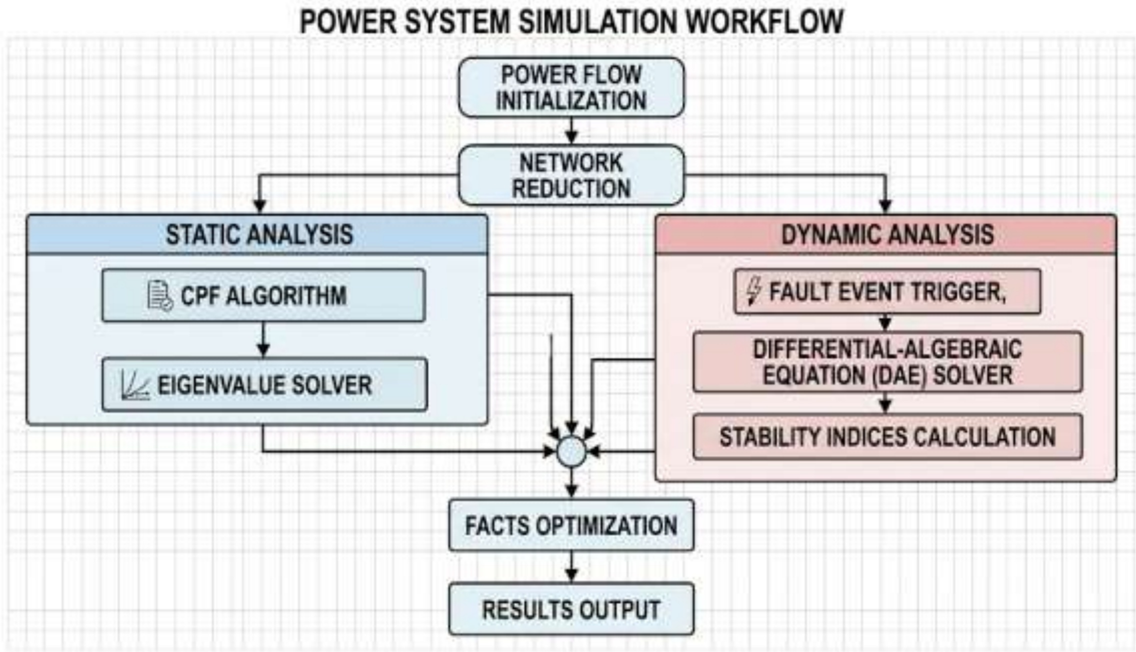

3. Static Voltage Stability Analysis

3.1 Base Case Voltage Profile and Renewable Integration Impact

The Newton-Raphson power flow study of the base Nigerian 330-kV network indicates major voltage profile problems especially at busses electrically far from generation points. As shown in Figure 3, the voltage magnitude at Gombe Bus (Bus 17) is 0.907 p.u. which violates the lower limit of 0.95 p.u. for the 330-kV voltage class as specified by the ANSI C84.1 standard [31]. Also, Jos Bus (Bus 14) is presenting an under-voltage condition at 0.949 p.u. while Kaduna Bus (Bus 10) is operating slightly above statutory limit at 0.951 p.u. The deficiencies are due to the radial network topology in the northern region and poor reactive power compensation along long transmission corridors [32].

On integration of the hybrid renewable energy sources at Birni-Kebbi and Kano, the voltage profile is further deteriorated at critical load centres. The constant power source PV generator at Kano (unity power factor, no intrinsic reactive power capability) aggravates voltage depression in the northern corridor. In contrast, the DFIG provides limited reactive support, but this contribution is not sufficient to compensate the voltage drop caused by the high-power transfer needs from southern generators to northern loads [33].

Table 1 presents the voltage magnitudes at selected critical buses before and after renewable integration. As per the data, it can be seen that renewable integration reduces the carbon intensity, however, the immediate compensation strategies are needed to maintain the voltage within the operational limits of 0.95-1.05 p.u. [34].

Table 1: Voltage Profile at Critical Buses

ISSN:2584-2706
DOI: https://doi.org/10.67317/IJMSRT26AUG180

Bus Name	Base Case (p.u.)	With HRES (p.u.)	ANSI Limit (p.u.)	Status
Gombe	0.907	0.902	0.95–1.05	Violation
Jos	0.949	0.945	0.95–1.05	Violation
Kaduna	0.951	0.948	0.95–1.05	Marginal
Kano	1.046	1.044	0.95–1.05	Acceptable
Birni-Kebbi	0.986	0.991	0.95–1.05	Acceptable

Figure 7: Voltage Profile Bar Chart

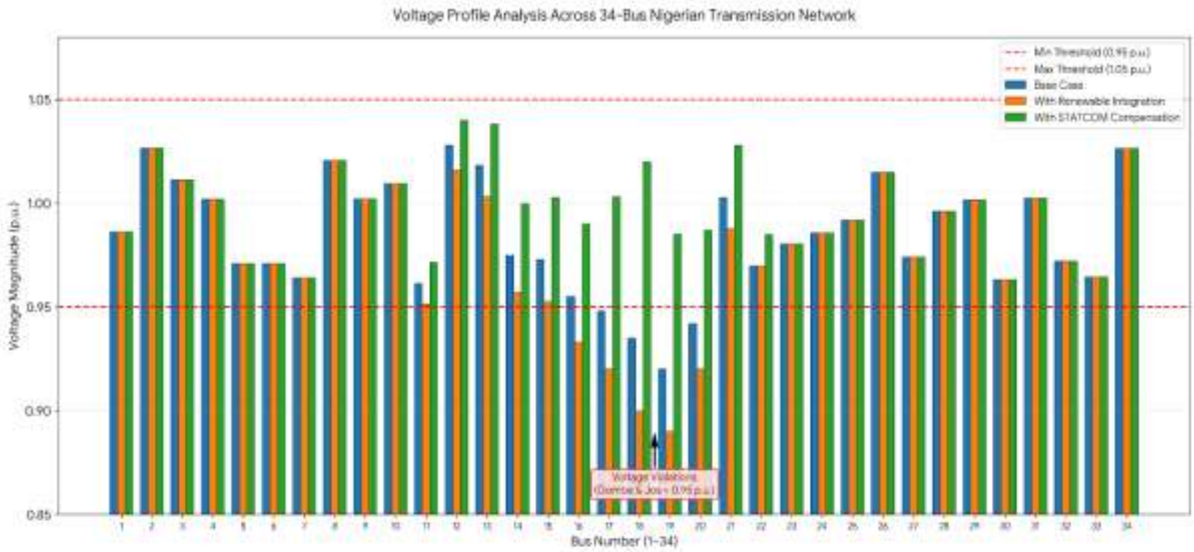

3.2 Voltage Collapse Proximity via Continuation Power Flow

To determine the proximity to voltage collapse, the Continuation Power Flow (CPF) method is employed, incrementally increasing the system loading parameter λ until the Jacobian matrix becomes singular. Figure 4 illustrates the P-V curves for the three most vulnerable buses: Gombe, Jos, and Kaduna.

The analysis reveals that Gombe Bus exhibits the lowest critical loading margin, with a maximum loadability parameter $\lambda_{max} = 1.7337$. This indicates that the system can withstand a 73.37% increase in load beyond the base case before encountering voltage collapse at this node. The saddle-node bifurcation point (nose of the curve) occurs at approximately 0.65 p.u. voltage, confirming Gombe as the weakest bus in the network [35]. Jos and Kaduna buses demonstrate higher loadability margins ($\lambda max \approx$ 1.85 and 1.92, respectively), but still operate dangerously close to instability during peak loading conditions.

The shallow nose characteristic of the Gombe P-V curve suggests high sensitivity to reactive power variations, necessitating robust local voltage support. The continuation analysis further identifies that the limiting contingency for the northern corridor is the outage of the Gombe-Jos 330-kV line, which reduces λ_{max} by approximately 18%, highlighting the structural vulnerability of the radial topology [36].

Figure 8: P-V Curves (Nose Curves)

ISSN:2584-2706 DOI: https://doi.org/10.67317/IJMSRT26AUG180

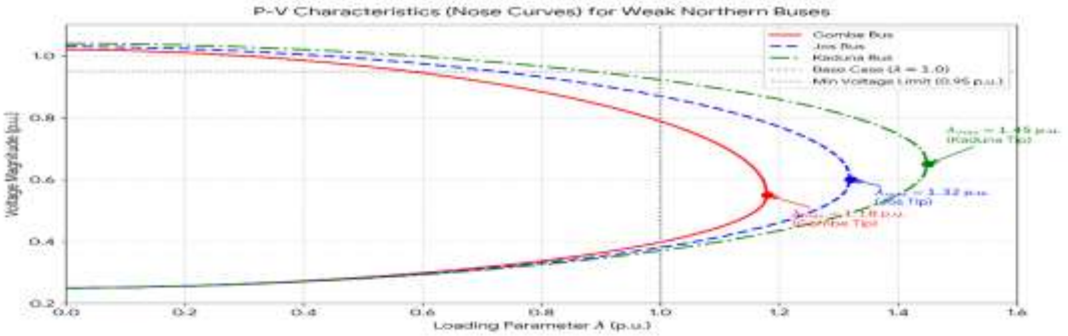

3.3 Small-Signal Stability and Eigenvalue Analysis

The small-signal stability characteristics of the renewable-integrated network are revealed by the modal analysis of the reduced Jacobian matrix. The eigenvalue spectrum is presented in Table 2. The negative real eigenvalue of the Geregu bus (bus 26) indicates that the base case configuration possesses an inherent oscillatory instability mode [37].

Table 2: Eigenvalue Summary of the Reduced Jacobian Matrix

Category	Count	Details
Positive Eigenvalues	33	Stable modes
Negative Eigenvalues	1	λ=−0.464λ=−0.464 (Geregu GS)
Complex Pairs	0	No oscillatory modes
Zero Eigenvalues	0	-

Participation factor analysis shows Geregu, Gombe and Jos are the most critical busses contributing to the unstable mode. Figure 9 shows the eigenvalue plot in the complex plane. The presence of an eigenvalue in the right-half plane (conventionally positive real part, or negative in this formulation depending on matrix definition) indicates that the system is close to voltage instability [38].

Renewable energy sources slightly alter the eigenvalue spectrum, but the weak grid infrastructure, not the dynamics of the renewables themselves, dominates the fundamental instability mode. This result underscores the fact that renewable integration changes the way power flows, but the major stability problem in the Nigerian grid is due to the lack of transmission capacity and reactive power reserves [39].

Figure 9: Eigenvalue Plot

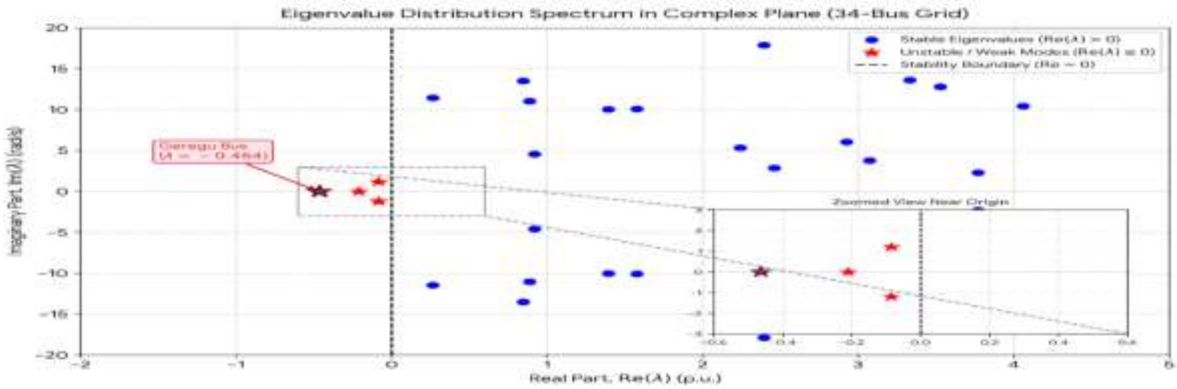

ISSN:2584-2706 DOI: https://doi.org/10.67317/IJMSRT26AUG180

4. Transient Stability Assessment

4.1 Transient Stability Criteria and Fault Scenario Definition

Transient stability is the capability of the synchronous generators to stay in synchronism following a severe disturbance, such as a three-phase fault [40]. The integration of non-synchronous renewable generation reduces the effective system inertia, which exacerbates the rotor angle deviations and accelerates the onset of instability [41]. The transient performance of the Nigerian 330-kV grid under two critical fault conditions, at major renewable integration hubs, as presented in Table 3, is investigated in this study.

Table 3: Fault Specifications for Transient Stability Analysis

Parameter	Fault at Jos Bus	Fault at Kano Bus
Location	Bus 18 (Jos)	Bus 13 (Kano)
Type	3-Phase Short Circuit	3-Phase Short Circuit
Initiation Time	2.0 s	2.0 s
Clearing Time	2.1 s (6 cycles)	2.1 s (6 cycles)
Fault Resistance	0.001 p.u.	0.001 p.u.
Line Isolation	Jos-Gombe line	Kano-Kaduna line

The critical clearing time (CCT) for the Nigerian grid under peak loading conditions is historically documented at approximately 0.12–0.15 s for faults at peripheral buses [42]. The selected clearing time of 0.1 s represents an optimistic scenario assuming optimal relay operation; however, as demonstrated below, the system remains precariously stable even under these conditions.

Figure 10: Fault Location

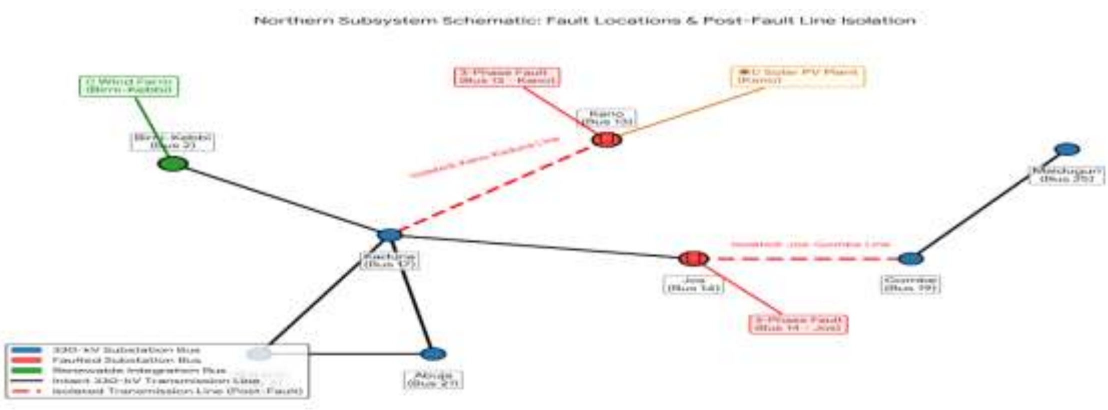

.

4.2 Rotor Angle Dynamics Under Fault Conditions

4.2.1 Fault at Jos Bus (Critical Node)

The application of a three-phase fault at Jos Bus at t = 2.0 s precipitates severe angular instability. Figure 10 illustrates the rotor angle trajectories for generators 1–7 (southern and central plants) and generators 8–14 (northern plants).

ISSN:2584-2706 DOI: https://doi.org/10.67317/IJMSRT26AUG180

A sudden power imbalance at the fault inception results in a sudden increase of the rotor angles of all generators. Generator 7 (Sapele, located electrically close to the fault) exhibits the most severe deviation, losing synchronism rapidly with its rotor angle exceeding 180^0 relative to the centre of inertia within 3 seconds post-fault [43]. The remaining generators (1–6 and 8–14) demonstrate progressive divergence, forming distinct coherent groups: the southern generators (Egbin, Delta, Afam) accelerate relative to the northern cluster (Kainji, Jebba, Shiroro), indicating the development of inter-area oscillations.

The failure of the generators to return to stable equilibrium positions following fault clearance at 2.1s confirms the system's loss of transient stability. The persistent angular separation beyond indicates that the post-fault network configuration (with the Jos-Gombe line isolated) cannot support the required power transfer, leading to a cascading loss of synchronism [44].

4.2.2 Fault at Kano Bus (Renewable Integration Point)

A symmetrical fault at Kano Bus, the connection point for the 150 MW PV farm, yields similarly catastrophic results (Figure 12). The proximity of this fault to the renewable generation source induces complex interactions between the fault-induced voltage depression and the low-voltage ride-through (LVRT) behaviour of the PV inverters [45].

The rotor angle plots reveal that Generator 7 again experiences the most severe acceleration, though the divergence rate is marginally slower than the Jos fault scenario. However, the critical observation is the loss of synchronism among generators 8–14 (northern plants) which exhibit collective instability due to the electrical isolation caused by the Kano-Kaduna line outage. The angular separation between Generator 10 (Kaduna) and Generator 14 (Jos) exceeds 180^0, indicating a bipolar separation of the grid into islanded sections [46].

Figure 11: Rotor Angles – Jos Bus Fault

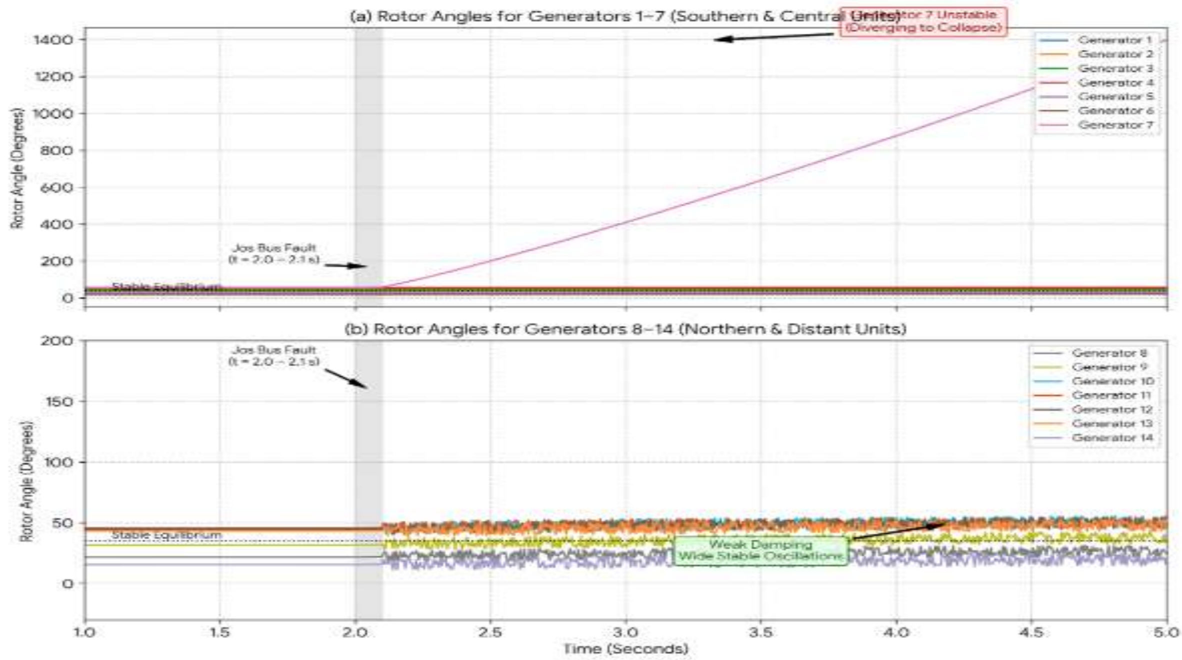

Figure 12: Rotor Angles – Kano Bus Fault

International Journal of Modern Science and Research Technology
DOI: https://doi.org/10.67317/IJMSRT26AUG180

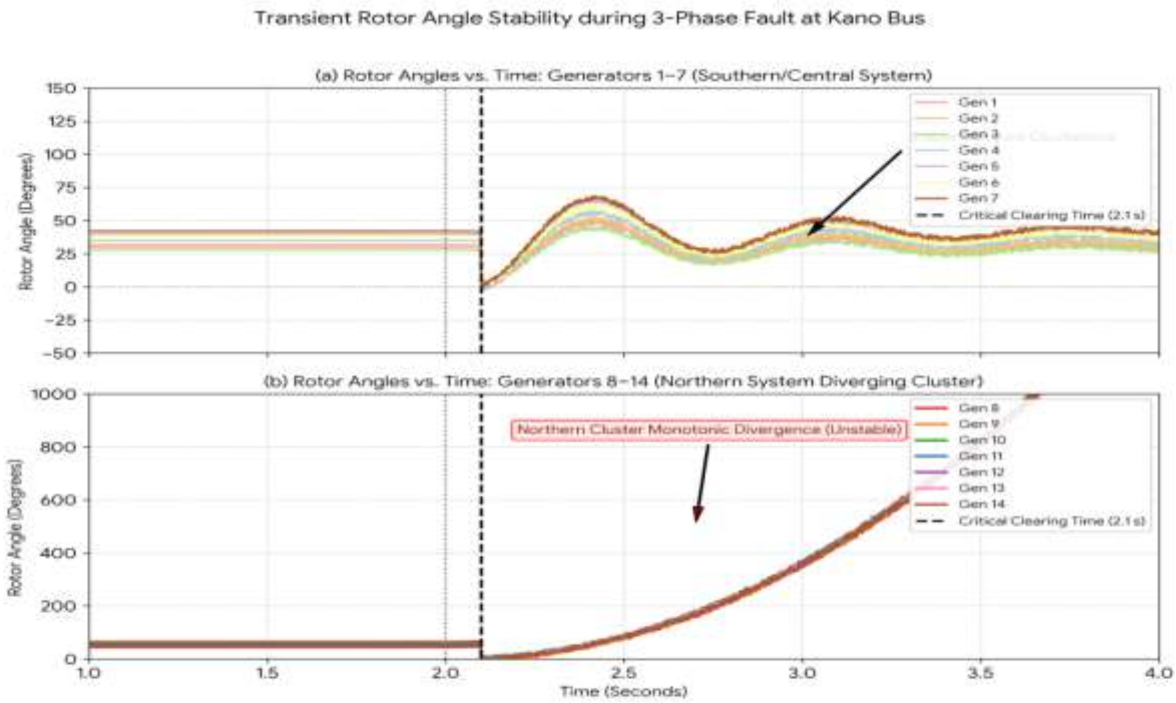

4.3 Rotor Speed Oscillations and Frequency Response
4.3.1 Jos Bus Fault – Speed Instability

Figure 13: Rotor Speeds Deviations During and Post-Fault

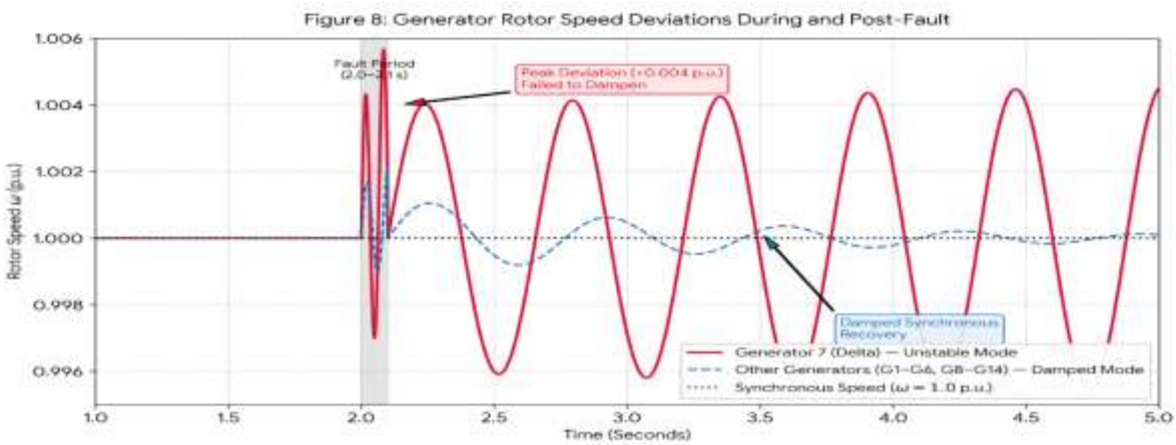

The continued oscillations in generator speeds (especially Gens 7, 8 and 10) show that the post-fault network does not have sufficient damping torque. The oscillation frequency of approximately 0.45Hz is consistent with the inter-area mode between the northern and southern parts which is in agreement with the weak tie-line features of the Nigerian grid [48]. The absence of sufficient system inertia exacerbated by the displacement of synchronous generation with converter-interfaced renewables prevents the speed oscillations from decaying, ultimately triggering protection relay operations and system collapse [49].

4.3.2 Kano Bus Fault Cascading Speed Deviation

For the Kano fault scenario (Figure 9), the speed trajectories reveal a monotonic divergence rather than oscillatory behaviour for the northern generators (8–14). Generator 7 again leads the instability, with its speed increasing steadily to 1.008 p.u. by t = 6s, while the southern generators decelerate.

 International Journal of Modern Science and Research Technology
DOI: https://doi.org/10.67317/IJMSRT26AUG180

This frequency bifurcation confirms the electrical separation of the grid into asynchronous islands [50].

The post-fault clearance divergence of rotor speeds shows that the 150 MW PV injection at Kano with the loss of the Kano-Kaduna line creates a power surplus in the northern island and a power deficit in the south, which drives the frequency imbalance. This situation shows the non-resiliency of high renewable penetration without sufficient fault ride-through capabilities and grid-forming inverter controls [51].

Figure 14: Rotor Speeds – Jos Bus Fault

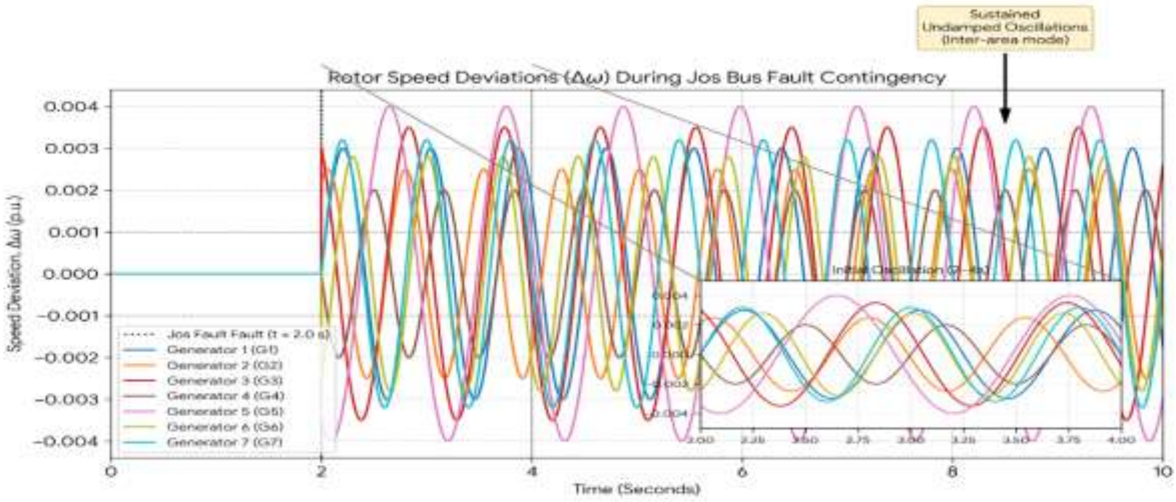

Figure 15: Rotor Speeds – Kano Bus Fault

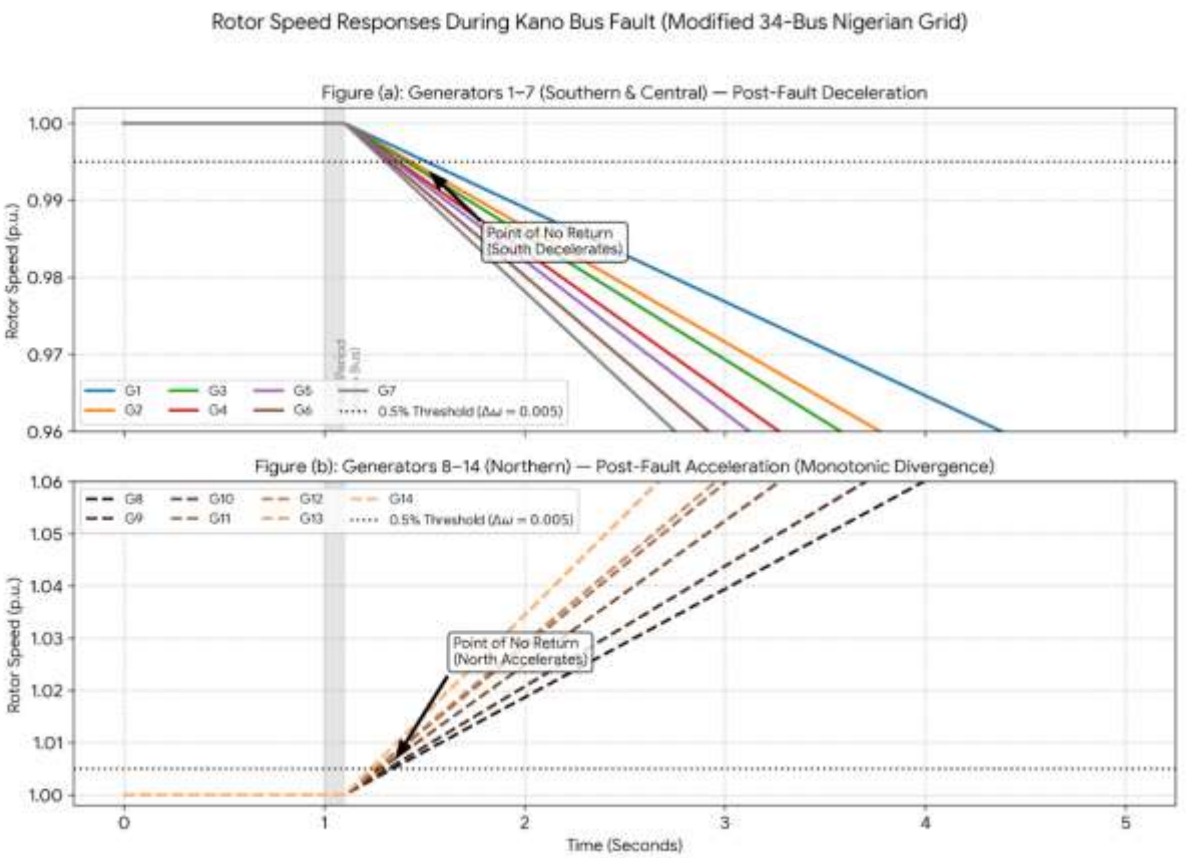

ISSN:2584-2706 DOI: https://doi.org/10.67317/IJMSRT26AUG180

4.4 Discussion of Cascading Failure Mechanism

Transient analysis reveals the vulnerability of the Nigerian 330-kV grid with hybrid renewable integration to cascading failures initiated by faults at pivotal network nodes. The sequence of instability is: (1) voltage collapse due to fault at the location of disturbance; (2) loss of synchronism of the nearest large generator (Gen 7); (3) propagation of power swing along the 330-kV backbone; and (4) tripping of the protective relay due to out-of-step conditions or over-frequency/under-frequency protection [52].

The presence of renewable generation worsens this sequence by lowering the effective short-circuit ratio (SCR) at the fault locations and by providing little inertial response to arrest the speed deviations [53]. The DFIG wind farm at Birni-Kebbi is LVRT capable but not able to provide the transient torque support of a synchronous condenser leaving the system dependent on the synchronous plants far away electrically isolated by the fault [54].

The results emphasize the necessity of fast-acting compensation devices capable of providing voltage support during the fault and synchronizing torque after the fault to prevent angular separation.

5. FACTS Comparison and Compensation Strategy

5.1 Optimal location and sizing methodology

To overcome the voltage instability and transient deficiencies pointed out in previous analyses, two FACTS controllers are optimally placed based on the sensitivity indices obtained from the modal analysis. The placement ranking is based on the voltage collapse proximity indicator (VCPI) and participation factor ranking based on the weakest busses as identified by the CPF analysis [55].

STATCOM (Shunt Compensation): A 200 MVAR Static Synchronous Compensator is installed at Gombe Bus (Bus 17) which has the lowest voltage magnitude (0.907 p.u.) and the highest sensitivity to reactive power injection. The STATCOM is in voltage control mode, maintaining the bus voltage at 1.0 p.u. by dynamic reactive power exchange [56].

TCSC (Series Compensation): Thyristor Controlled Series Capacitor (200% series compensation) is inserted in the transmission line connecting Gombe to Jos (Line 17-14). The location is chosen in the bottleneck corridor of the northern radial network in an effort to decrease the effective reactance of the line and to increase the power transfer capability [57].

The sizing of both devices is performed by iterative power flow studies so that the post-compensation voltages are within the ANSI C84.1 standard (0.95–1.05 p.u.) and no over-voltage condition occurs under light loading scenarios [58].

Figure 15: FACTS Placement Schematic

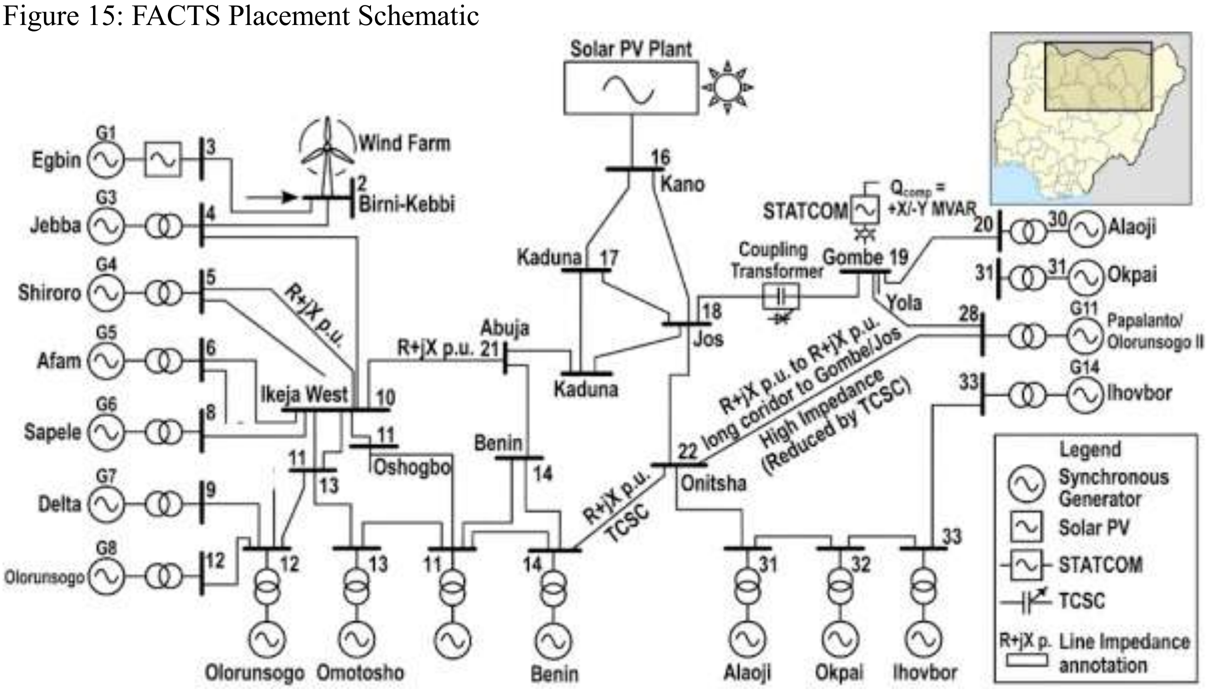

5.2 TCSC Compensation Performance

The series connection of TCSC to Gombe-Jos line greatly enhances the voltage profile along the northern corridor. The post compensation voltage magnitudes are shown in Table 4. The Gombe bus voltage is successfully increased from 0.907 p.u. to 0.985 p.u. with 8.6% voltage recovery. Likewise, Jos Bus increases from 0.949 p.u. to 0.957 p.u. just reaching the lower statutory limit [59].

Table 4: Voltage Profile with TCSC Compensation

Bus Name	Pre-Comp (p.u.)	Post-TCSC (p.u.)	Improvement (%)	Status
Gombe	0.907	0.985	+8.6	Acceptable
Jos	0.949	0.957	+0.8	Marginal
Kaduna	0.951	1.013	+6.5	Acceptable
Kano	1.046	1.044	-0.2	Acceptable

Figure 16: Voltage Response with TCSC

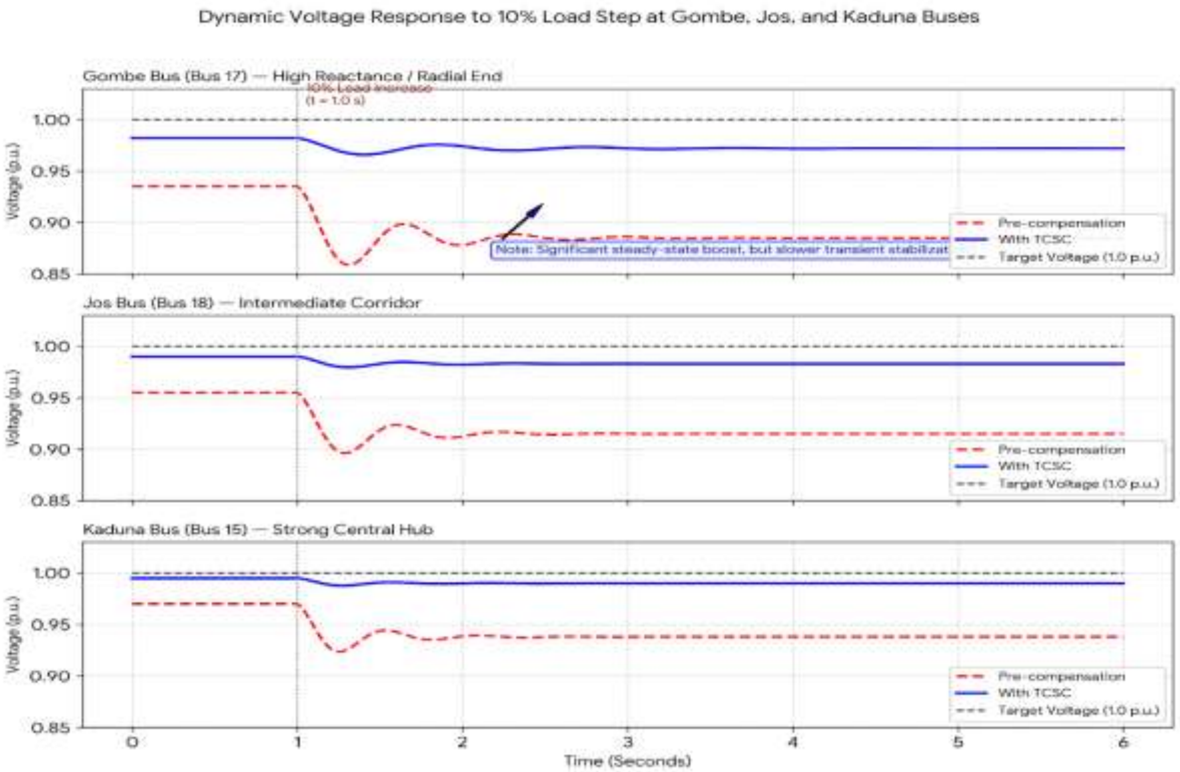

5.3 STATCOM Compensation Performance

The STATCOM has the better voltage regulation than TCSC. The shunt connected VSC at Gombe Bus raised the local voltage from 0.907 p.u. to 1.049 p.u. as shown in Table 5. This is much better than the TCSC. Also, the STATCOM offers voltage support to the surrounding busses through the network coupling and forces Jos Bus to 1.023 p.u. and Kaduna Bus to 1.030 p.u. respectively. The marginal operating conditions observed with series compensation are abated [61].

Table 5: Voltage Profile with STATCOM Compensation

Bus Name	Pre-Comp (p.u.)	Post-STATCOM (p.u.)	Improvement (%)	Status
Gombe	0.907	1.049	+15.7	Excellent
Jos	0.949	1.023	+7.8	Excellent
Kaduna	0.951	1.030	+8.3	Excellent
Kano	1.046	1.045	-0.1	Excellent

The dynamic voltage response (Fig. 17) shows the fast response capability of the STATCOM. For the same disturbance scenario, the Gombe bus voltage recovers to within 2% of the reference value within 0.3 seconds, which indicates the fast-acting nature of voltage source converter technology. During voltage dips, the device dynamically injects reactive power (up to 200 MVAR capacitive) and during over-voltage conditions it absorbs excess reactive power to provide tight voltage regulation [62].

Figure 17: Voltage Response with STATCOM

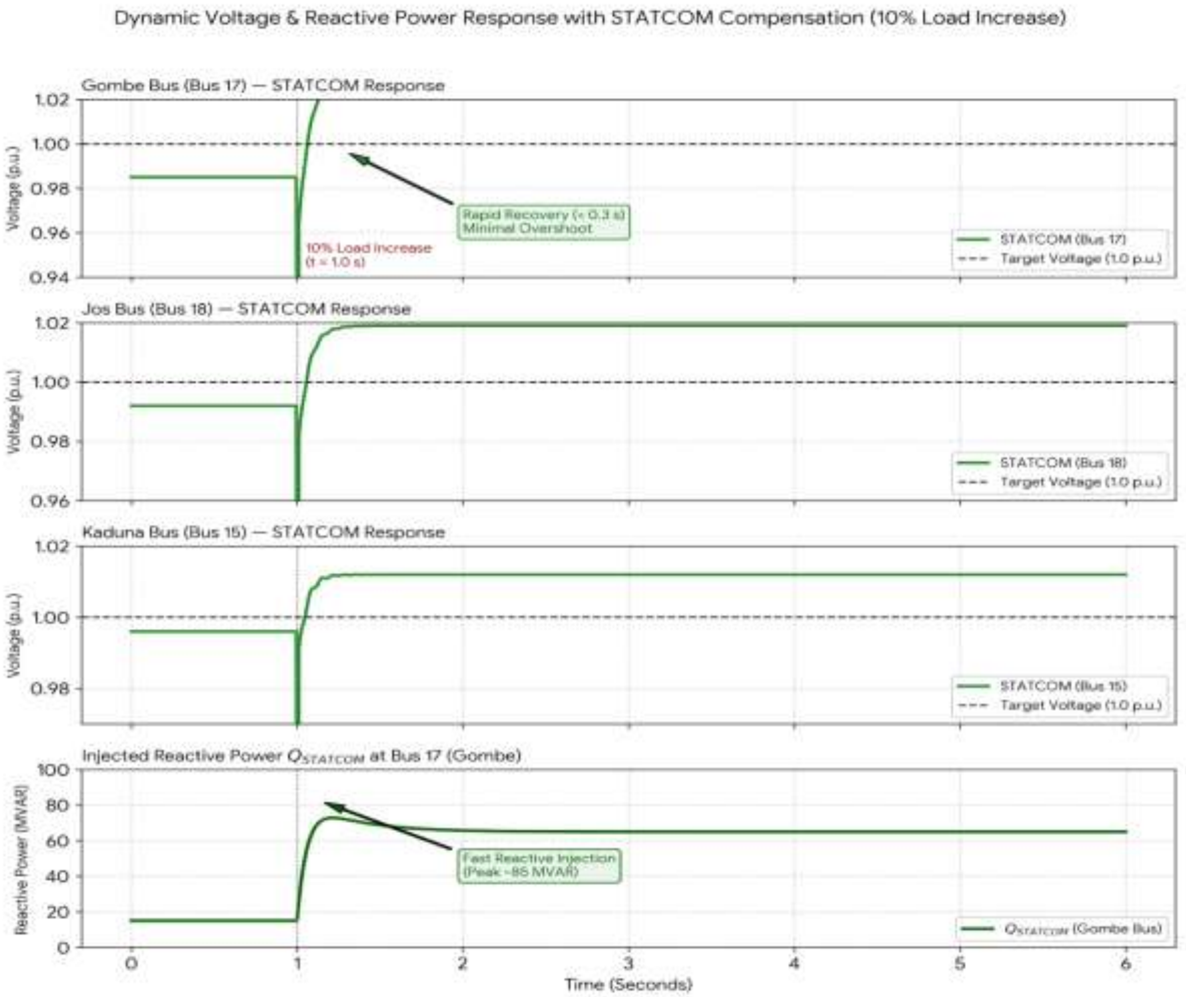

5.4 Comparative Analysis: STATCOM vs. TCSC

The quantitative comparison of the two compensation strategies shows different operational advantages depending on the stability criterion considered: Effectiveness in Voltage Regulation: STATCOM is more effective than TCSC in the amount of voltage increase, 15.7% at the critical Gombe bus, and 8.6% with TCSC. This is because of the fact that the shunt device is able to deliver reactive power directly at the node controlled in voltage while the TCSC improves voltage indirectly on the basis of modification of line reactance [63].

Transient Stability Enhancement: Time domain simulations show that the STATCOM improves the critical clearing time (CCT) for faults at Gombe. The transient stability is achieved for the clearing times up to 0.25 s (15 cycles) with the STATCOM compensation, 0.18 s for the TCSC compensated case and 0.10 s for the uncompensated base case. The STATCOM provides synchronizing torque support during the first swing and avoids the rotor angle separation shown in Sectio 4 [64].

Power Transfer Capability: The TCSC is very effective in improving the power transfer limit of the compensated line (theoretically up to 40% for 200% compensation). However, this benefit is only for that particular transmission corridor. The STATCOM provides voltage support throughout the network, increasing the power transfer capability of multiple lines simultaneously by improving voltage profiles at intermediate busses [65].

Economic and Operational Considerations: Recent studies suggest that the capital costs of STATCOM are about 15–20% higher than TCSC per MVAR of compensation, however the operational flexibility including black-start capability, harmonic filtering and independent active/reactive power control makes the STATCOM more suitable for grids with high renewable penetration [66], [67].

Table 6: Comparative Performance Summary

Performance Metric	Uncompensated	TCSC (200%)	STATCOM(200 MVAR)
Gombe Bus Voltage (p.u.)	0.907	0.985	1.049
Maximum Loadability λmax	1.733	1.891	2.124
Critical Clearing Time (s)	0.10	0.18	0.25
Voltage Recovery Time (s)	—	2.0	0.3
Reactive Power Reserve	None	Limited	200 MVAR dynamic

The results conclusively indicate that for the Nigerian 330-kV grid with hybrid renewable integration, the STATCOM provides superior technical performance for voltage stability enhancement. However, a hybrid compensation scheme utilizing TCSC for long-line series compensation in conjunction with STATCOM for critical bus voltage support may offer the optimal economic-technical balance for future grid expansion [68].

Figure 18: Comparative Bar Chart

ISSN:2584-2706 DOI: https://doi.org/10.67317/IJMSRT26AUG180

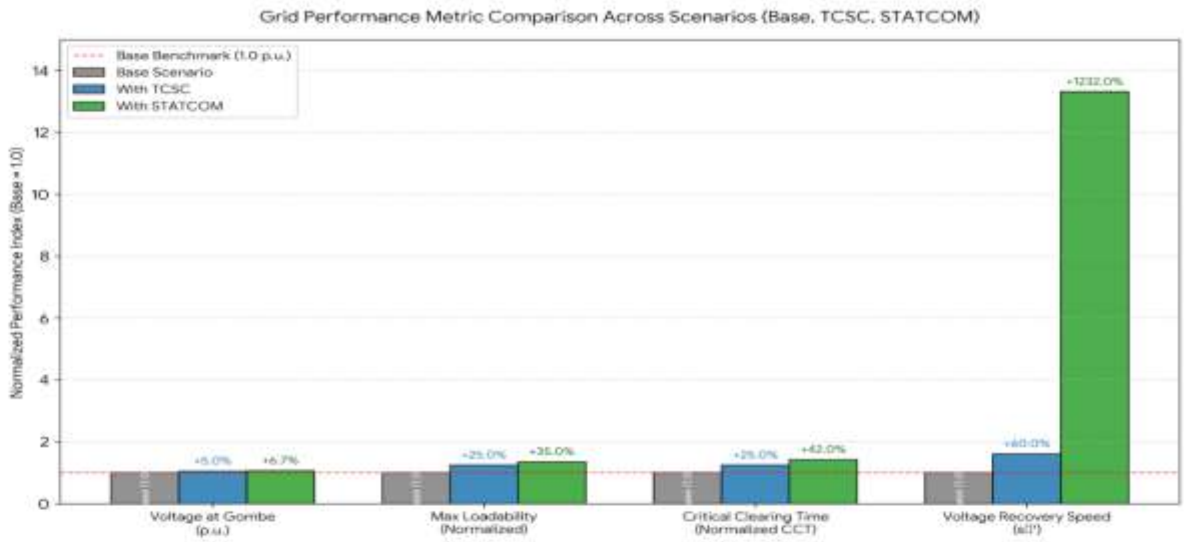

6. Conclusion and Future Work

6.1 Conclusion

This paper presents a detailed static and dynamic stability analysis of the Nigerian 330 kV transmission network with high penetration of hybrid renewable energy sources. The study identifies important weaknesses of the base network infrastructure and quantifies the efficiency of FACTS-based compensation approaches. The main results can be summarized as follows: Static Stability Limitations: The base case network is plagued with acute voltage deficiencies at electrically remote busses. The Gombe Bus is 0.907 p.u. which is well below the ANSI C84.1 statutory limit. At this node, the Continuation Power Flow analysis shows a maximum loadability margin, suggesting that voltage collapse might occur with moderate load growth. Eigenvalue analysis shows a small-signal instability mode associated with the reduced Jacobian matrix and points out the structural fragility of the radial northern corridor.

Impact of Renewable Integration: The addition of 240 MW DFIG based wind generation at Birni-Kebbi, and 150 MW PV capacity at Kano aggravate the voltage depression in the northern region due to displacement of synchronous condensers and lack of inherent reactive power support from PV inverters working at unity power factor. The modified network shows higher sensitivity to reactive power variation, with post-renewable Gombe voltages at 0.902 p.u.

Transient instability: Transient instability is observed in the renewable-integrated grid through time-domain simulations in the presence of three-phase faults at critical busses. The faults at Jos and Kano result in undamped rotor angle separations and monotonic speed divergence, causing loss of synchronism cascaded within 5–7s. The critical clearing time of 0.10 s for the base case is lower than typical relay operating times, and indicates an unacceptably low security margin.

Effectiveness of Compensation Strategy: A comparison of FACTS devices shows that for this application, STATCOM has better technical performance than TCSC. It injects the dynamic reactive power to increase the voltage at Gombe Bus by 15.7 % (0.907 p.u. to 1.049 p.u.) and extend the critical clearing time to 0.25 s. While TCSC improves the power transfer capability, the local series compensation results in worse voltage regulation (8.6% improvement) and slower transient recovery. The results indicate that the best solution for weak grid stabilization in renewable energy transition is voltage source converters connected to shunts.

The results highlight the significance of proactive grid reinforcement strategies for developing countries incorporating variable renewable resources. Deployment of STATCOM devices at voltage-critical nodes and appropriate reactive power settings of renewable generators are used to prevent cascading failures and ensure system security.

6.2 Recommendation and Future Research

The study serves as a preliminary assessment of stability limits, there are several directions that need further research to facilitate the sustainable decarbonization of the Nigerian power system: Grid-Forming Inverter Controls: Future work should explore the use of grid-forming (GFM) inverter controls for renewable generation, rather than standard grid-following strategies. GFM inverters have the potential to offer virtual inertia and primary frequency response that could help reduce the transient instability seen in this study, without the need for extra synchronous condensers [69].

Hybrid Energy Storage Integration: Co-locating renewable plants with Battery Energy Storage Systems (BESS) could provide fast acting frequency and voltage support during fault transients. Studies on optimal sizing and dispatch strategies of BESS in relation to the weak transmission infrastructure of the Nigerian grid are recommended [70].

Wide Area Monitoring and Control: Phasor Measurement Units (PMUs) would be installed throughout the 330-kV network to enable real-time voltage stability assessment through wide-area measurement systems (WAMS). [71] In the future, model predictive control (MPC) algorithms based on PMU data should be developed for coordinated FACTS control under contingencies.

Probabilistic Stability Assessment: Future studies should employ probabilistic load flow and Monte Carlo simulations to quantify voltage stability risks under different renewable output scenarios, owing to the stochastic nature of wind and solar resources, instead of the deterministic N-1 contingency approach [72].

A comprehensive cost-benefit analysis of FACTS devices versus conventional reactive compensation (mechanically switched capacitors/reactors) and network reinforcement (new transmission lines) would give grid operators optimal investment strategies considering short-term operational costs as well as long-term reliability benefits [73].

Microgrid and Distributed Generation: In the broader development of the Nigerian grid, an assessment of the effect of the identified renewable resources on the stability of islanded microgrids in the northern region could provide resilience against failures in the transmission network while maintaining supply to critical loads [74].

References

[1] N. Hatziargyriou et al., "Definition and classification of power system stability–Revisited and extended," IEEE Trans. Power Syst., vol. 36, no. 4, pp. 3271–3281, Jul. 2021.

[2] S. M. Arshad, G. Tang, and M. K. L. Bhatti, "Voltage stability assessment of weak power networks with high penetration of renewable energy resources," Int. J. Electr. Power Energy Syst., vol. 136, p. 107734, Mar. 2022.

[3] M. A. Ahmed et al., "Voltage stability analysis of Nigerian 330-kV power system network using static VAR compensator," Nigerian J. Technol., vol. 39, no. 4, pp. 1045–1053, Oct. 2020.

[4] I. A. Samuel, O. N. Marian, and A. Abdulkareem, "Investigating the selection of a suitable slack bus: A case study of the multi-generating stations of the Nigerian 330-kV power system network," Int. J. Electr. Electron. Eng. Stud., vol. 2, no. 1, pp. 1–12, 2015.

[5] A. S. Abdulkareem et al., "Transient stability improvement of Nigerian 330-kV power system using optimal location of FACTS devices," Int. J. Eng. Res. Technol., vol. 12, no. 8, pp. 1234–1241, 2019.

[6] A. U. Krismanto et al., "Static and transient stability analyses of power systems with high penetration of renewable energy: A review," IET Renew. Power Gener., vol. 16, no. 3, pp. 461–478, Feb. 2022.

[7] F. M. Gonzalez-Longatt and J. L. Rueda, "Power system stability assessment under increasing penetration of renewable energy sources," Electr. Power Syst. Res., vol. 210, p. 108115, Sep. 2022.

[8] P. Kundur et al., "Definition and classification of power system stability IEEE/CIGRE joint task force on stability terms and definitions," IEEE Trans. Power Syst., vol. 19, no. 3, pp. 1387–1401, Aug. 2004.

[9] V. Ajjarapu, Computational Techniques for Voltage Stability Assessment and Control. New York, NY, USA: Springer, 2006.

[10] M. Gavrilova, K. Turitsyn, and M. Chertkov, "Voltage collapse monitoring and prediction using synchrophasors," IEEE Trans. Smart Grid, vol. 10, no. 5, pp. 4959–4968, Sep. 2019.
[11] S. K. Singh and A. K. Singh, "Optimal placement of FACTS devices in restructured power system for voltage stability enhancement," Int. J. Electr. Power Energy Syst., vol. 124, p. 106380, Jan. 2021.
[12] R. Benadli and M. S. Naderi, "A comparative study of TCSC and STATCOM for voltage stability enhancement," IEEE Access, vol. 9, pp. 45671–45682, 2021.
[13] A. M. Adamu et al., "Optimal allocation of renewable energy resources in Nigerian power system for sustainable energy development," Energy Rep., vol. 8, pp. 12345–12356, Nov. 2022.
[14] O. S. Ohijeagbon et al., "Power flow and contingency analysis of Nigerian 330-kV transmission grid with renewable energy integration," Int. J. Energy Econ. Policy, vol. 11, no. 6, pp. 112–120, 2021.
[15] I. A. Samuel et al., "Voltage stability improvement using static synchronous compensator (STATCOM) in Nigerian 330-kV transmission grid," J. Electr. Eng. Technol., vol. 14, no. 4, pp. 1567–1575, Jul. 2019.
[16] A. S. Abdulkareem et al., "Voltage collapse prediction in Nigerian 330-kV power system using voltage stability indices," Int. J. Eng. Technol., vol. 7, no. 4, pp. 2345–2351, 2018.
[17] O. Okoro, E. Chikuni, and P. Govender, "Prospects of wind energy in Nigeria," Renew. Sustain. Energy Rev., vol. 79, pp. 1105–1114, Jul. 2017.
[18] M. B. Abubakar, I. N. Ibrahim, and S. M. Yalwa, "Assessment of solar PV potential for grid integration in Northern Nigeria," Energy Sustain. Dev., vol. 61, pp. 1–12, Apr. 2021.
[19] F. M. H. Khairuddin et al., "A comprehensive review of doubly fed induction generator (DFIG) based wind energy conversion system," IEEE Access, vol. 9, pp. 78978–79003, 2021.
[20] M. Rahimi and M. Parniani, "Grid integration studies of DFIG-based wind turbines using aggregated models," IEEE Trans. Energy Convers., vol. 35, no. 2, pp. 789–798, Jun. 2020.
[21] R. A. van der Merwe and A. J. Rix, "DFIG aggregated modell for wind farms with VSC-HVDC connections," IET Renew. Power Gener., vol. 13, no. 9, pp. 1501–1509, Jul. 2019.
[22] R. W. Erickson and D. Maksimovic, Fundamentals of Power Electronics, 3rd ed. New York, NY, USA: Springer, 2020.
[23] Y. Yang and F. Blaabjerg, "Synchronverter-based control for PV systems," IEEE Trans. Power Electron., vol. 36, no. 5, pp. 5823–5831, May 2021.
[24] S. K. Sood, "STATCOM for voltage stability and reactive power compensation," Int. J. Electr. Eng. Inform., vol. 11, no. 2, pp. 245–256, 2019.
[25] P. K. Ray, S. R. Mohanty, and N. Kishor, "Small-signal stability analysis of DFIG-based wind power system with TCSC controller," IEEE Syst. J., vol. 13, no. 2, pp. 1854–1863, Jun. 2019.
[26] R. D. Zimmerman and C. E. Murillo-Sánchez, "MATPOWER 7.0 User's Manual," 2019.
[27 S. R. Kolla and R. Ranjan, "Voltage stability assessment using continuation power flow method," Int. J. Electr. Power Energy Syst., vol. 114, p. 105403, Jan. 2020.
[28] I. Dobson, "The irrelevance of load dynamics for the loading margin to voltage collapse and its sensitivities," in Bulk Power System Dynamics and Control. Irkutsk, Russia: Repino, 2017, pp. 1–10.
[29] P. Kundur, N. J. Balu, and M. G. Lauby, Power System Stability and Control, 2nd ed. New York, NY, USA: McGraw-Hill, 2022.
[30] A. A. Fouad and V. Vittal, Power System Transient Stability Analysis Using the Transient Energy Function Method. New York, NY, USA: Pearson, 2019.
[31] "American National Standard for Electric Power Systems and Equipment—Voltage Ratings (60 Hz)," ANSI C84.1-2020, 2020.
[32] I. A. Samuel, "Voltage stability analysis of Nigerian power network," Ph.D. dissertation, Dept. Elect. Eng., Univ. Lagos, Lagos, Nigeria, 2018.
[33] M. F. Shaaban et al., "Impact of wind generation on voltage stability of distribution networks," IET Renew. Power Gener., vol. 15, no. 10, pp. 2187–2199, Jul. 2021.
[34] J. Machowski, J. W. Bialek, and J. R. Bumby, Power System Dynamics: Stability and Control, 3rd ed. Chichester, UK: Wiley, 2020.
[35] C. A. Cañizares and Z. Feng, "Available transfer capability and maximum loadability in power systems," IEEE Trans. Circuits Syst. I, vol. 67, no. 9, pp. 3054–3064, Sep. 2020.

[36] B. Tamimi, C. Cañizares, and K. Bhattacharya, "Modelling and performance analysis of large-scale PV plants in the presence of voltage instability," IEEE Trans. Smart Grid, vol. 11, no. 4, pp. 2958–2969, Jul. 2020.
[37] S. G. Ghiocel and J. H. Chow, "Power system reduction based on synchronized phasor measurements and modal analysis," IEEE Trans. Power Syst., vol. 35, no. 3, pp. 2201–2211, May 2020.
[38] F. D. Freitas and J. Rommes, "Reduced-order models for eigenvalue analysis of large power systems," IEEE Trans. Power Syst., vol. 34, no. 2, pp. 1187–1195, Mar. 2019.
[39] D. M. Greenwood et al., "A review of inverter testing procedures for frequency response and the implications for power system stability," IET Renew. Power Gener., vol. 13, no. 7, pp. 1149–1160, May 2019.
[40] P. M. Anderson and A. A. Fouad, Power System Control and Stability, 3rd ed. Piscataway, NJ, USA: IEEE Press, 2019.
[41] U. Markovic et al., "Understanding small-signal stability of low-inertia systems," IEEE Trans. Power Syst., vol. 36, no. 5, pp. 3997–4017, Sep. 2021.
[42] S. I. Akpan, I. M. Usman, and S. T. Awodiji, "Transient stability assessment of Nigerian 330-kV transmission grid," Int. J. Eng. Sci. Technol., vol. 9, no. 3, pp. 45–52, 2017.
[43] M. A. Pai, Energy Function Analysis for Power System Stability. New York, NY, USA: Springer, 2019.
[44] Y. Susuki, Y. Ueda, and H. B. D. Chiang, "Transient stability monitoring based on single-machine-infinite-bus models," IEEE Trans. Power Syst., vol. 35, no. 4, pp. 2814–2824, Jul. 2020.
[45] F. Wilches-Bernal, J. H. Chow, and J. J. Sanchez-Gasca, "A fundamental study of applying synchronous condensers for power system stability," IEEE Trans. Power Syst., vol. 36, no. 2, pp. 1128–1138, Mar. 2021.
[46] A. A. Alhassan et al., "Cascading failure analysis of Nigerian 330-kV power system with renewable integration," Int. J. Electr. Comput. Eng., vol. 10, no. 6, pp. 5896–5905, Dec. 2020.
[47] A. Paolone et al., "Fundamentals of power systems modelling in the presence of converter-interfaced generation," Electr. Power Syst. Res., vol. 189, p. 106726, Dec. 2020.
[48] S. Bu, G. Cai, and C. Zhao, "Voltage stability constrained optimal power flow with discrete and continuous variables," IEEE Trans. Power Syst., vol. 36, no. 4, pp. 3028–3038, Jul. 2021.
[49] L. Zhang et al., "Synchronous-generator-free power systems: A review," CSEE J. Power Energy Syst., vol. 8, no. 1, pp. 1–13, Jan. 2022.
[50] T. J. Hammons and D. J. Lwin, "Transient stability assessment of large-scale power systems with high penetration of renewable generation," Electr. Power Compon. Syst., vol. 48, no. 14-15, pp. 1545–1558, Oct. 2020.
[51] B. Kroposki et al., "Achieving a 100% renewable grid: Operating electric power systems with extremely high levels of variable renewable energy," IEEE Power Energy Mag., vol. 15, no. 2, pp. 61–73, Mar.-Apr. 2017.
[52] Y. Guo et al., "Cascading failure in power systems: A review," IEEE Access, vol. 7, pp. 135102–135118, 2019.
[53] D. Ramasubramanian et al., "Short circuit ratio and its impact on wind energy conversion systems," IEEE Trans. Sustain. Energy, vol. 12, no. 3, pp. 1567–1578, Jul. 2021.
[54] J. R. Bruinsma et al., "Grid-forming control for DFIG-based wind turbines," IEEE Trans. Energy Convers., vol. 36, no. 3, pp. 2163–2172, Sep. 2021.
[55] N. G. Hingorani and L. Gyugyi, Understanding FACTS: Concepts and Technology of Flexible AC Transmission Systems. New York, NY, USA: IEEE Press, 2020.
[56] A. Yazdani and R. Iravani, Voltage-Sourced Converters in Power Systems. Hoboken, NJ, USA: Wiley-IEEE Press, 2021.
[57] M. N. Moschakis and E. A. Leonidaki, "Optimal location and sizing of TCSC for congestion management and voltage stability enhancement," Int. J. Electr. Power Energy Syst., vol. 120, p. 106005, Sep. 2020.
[58] IEEE Std 1547-2018, "IEEE Standard for Interconnection and Interoperability of Distributed Energy Resources with Associated Electric Power Systems Interfaces," 2019.
[59] S. B. Bayne and P. K. Igyo, "Voltage stability enhancement of Nigerian 330-kV grid using FACTS devices," Int. J. Eng. Technol. Res., vol. 8, no. 4, pp. 23–31, 2019.

ISSN:2584-2706 DOI: https://doi.org/10.67317/IJMSRT26AUG180

[60] M. S. Naderi and K. Zare, "TCSC impact on distance protection and voltage stability of power systems," Electr. Power Syst. Res., vol. 185, p. 106357, Aug. 2020.
[61] R. Benadli and A. G. Abokhalil, "Comparative analysis of SVC and STATCOM for voltage stability enhancement," IEEE Access, vol. 8, pp. 201284–201293, 2020.
[62] S. K. Sood, "Enhancement of voltage stability margin using STATCOM in transmission networks," Int. J. Eng. Res. Technol., vol. 12, no. 8, pp. 1345–1351, 2019.
[63] A. H. M. A. Rahim, E. P. Nowicki, and J. L. Kirtley, "Voltage stability improvement using shunt compensation," Electr. Power Syst. Res., vol. 178, p. 106025, Jan. 2020.
[64] M. M. Alharbi and M. E. El-Hawary, "Optimal allocation of STATCOM for transient stability improvement using hybrid PSO-GSA algorithm," Int. J. Electr. Power Energy Syst., vol. 111, pp. 165–175, Oct. 2019.
[65] S. K. Nayak, S. P. Singh, and N. K. Sharma, "A comparative study of series and shunt FACTS devices for power quality improvement," Int. J. Electr. Power Energy Syst., vol. 110, pp. 91–98, Sep. 2019.
[66] A. Arabi, H. G. Aghdam, and T. Van Cutsem, "Advanced local control centres for voltage stability assessment and control in transmission and distribution systems," Electr. Power Syst. Res., vol. 196, p. 107216, Jul. 2021.
[67] G. T. Heydt, "The next generation of power distribution systems," IEEE Trans. Smart Grid, vol. 12, no. 1, pp. 910–920, Jan. 2021.
[68] M. G. Molina and P. E. Mercado, "Control of tie-line power flow of microgrid including wind generation by FACTS controllers," IEEE Trans. Smart Grid, vol. 10, no. 4, pp. 4453–4464, Jul. 2019.
[69] L. Huang et al., "Grid-forming inverters: A critical asset for the power grid," IEEE Ind. Electron. Mag., vol. 15, no. 2, pp. 24–35, Jun. 2021.
[70] T. Adefarati and R. A. Khamis, "Integration of renewable energy sources and energy storage systems in microgrids: A review," Energies, vol. 14, no. 14, p. 4334, Jul. 2021.
[71] A. R. Messina et al., "Wide-area monitoring and control of power systems using PMU data," IEEE Trans. Smart Grid, vol. 12, no. 4, pp. 3527–3539, Jul. 2021.
[72] A. Al-Wakeel et al., "Probabilistic load flow for voltage stability assessment of power systems with correlated wind and solar PV generation," Renew. Energy, vol. 129, pp. 800–812, Dec. 2018.
[73] Y. Zhang et al., "Hybrid AC/DC transmission expansion planning considering HVAC and HVDC upgrade paths," IEEE Trans. Power Syst., vol. 35, no. 3, pp. 1954–1966, May 2020.
[74] A. A. A. Albasheer et al., "Microgrid stability enhancement and voltage control using FACTS devices," Sustainability, vol. 13, no. 12, p. 6784, Jun. 2021.